# Orientational Disorder of (trans)-4-Chloro-4 0 -nitrostilbene: A Detailed Analysis by Single Crystal X-ray Diffraction

**ARTICLE** *in* CRYSTAL GROWTH & DESIGN · JANUARY 2010

Impact Factor: 4.89 · DOI: 10.1021/cg801278j



**6 AUTHORS**, INCLUDING:

Gaël Charles Labat
École d'ingénieurs de Changins
**77** PUBLICATIONS **886** CITATIONS
SEE PROFILE

Venugopalan Paloth
Panjab University
**191** PUBLICATIONS **1,923** CITATIONS
SEE PROFILE

hans-beat Buergi
University of Zurich
**243** PUBLICATIONS **6,107** CITATIONS
SEE PROFILE

DOI: 10.1021/cg801278j

CRYSTAL GROWTH & DESIGN Article

2010, Vol. 10 52–59

# Orientational Disorder of (*trans*)-4-Chloro-4′-nitrostilbene: A Detailed Analysis by Single Crystal X-ray Diffraction

Norwid-Rasmus Behrnd,[†] Gaël Labat,[†,‡] Paloth Venugopalan,[‡,#] Jürg Hulliger,*[,†] and Hans-Beat Bürgi*[,‡]

[†]*Department of Chemistry and Biochemistry, University of Berne, Freiestrasse 3, CH-3012 Berne, Switzerland,* [‡]*Laboratory of Chemical Crystallography, University of Berne, Freiestrasse 3, CH-3012 Berne, Switzerland, and* [#]*Department of Chemistry, Panjab University, Chandigarh, 160 014 India*

*Received November 19, 2008; Revised Manuscript Received August 11, 2009*

**ABSTRACT:** A detailed X-ray diffraction study of (*trans*)-4-chloro-4′-nitrostilbene, which shows significant second-harmonic generation, revealed subtle deviations from the centrosymmetric structure reported earlier on the basis of a largely automated structure analysis. The deviations are due to unequal populations of disordered molecules superimposed in two opposite orientations across an inversion center. Weak superstructure reflections indicate a doubling of the unit cell leading to four disordered sites, each with a different imbalance of populations.

## 1. Introduction

Crystalline (*trans*)-4-chloro-4′-nitrostilbene (hereafter CNS) shows second harmonic generation (SHG) that is significant compared to urea. Its magnitude measured with solvent-free samples has been reported to depend on the solvent of crystallization.[1] A crystal structure analysis published thereafter reported the centrosymmetric space group $P2_1/c$, incompatible with the observation of SHG.[2]

New X-ray diffraction experiments on CNS crystallized from benzene revealed significant intensities of reflection that are forbidden in space group $P2_1/c$; in addition, weak superstructure reflections were observed at $h\ k+1/2\ l+1/2$ . These data are better interpreted in noncentrosymmetric space groups, thus resolving the contradiction between the observed SHG activity and the previous structure report. As the following discussion will show, the physical properties of this molecular crystal are the result of a complex interplay between orientational disorder at the level of molecular packing on one hand and twinning at a larger, difficult-to-determine length scale on the other (section 3.2). The influence of the solvent of crystallization on the disorder of this crystal structure will be described in a later publication.[3]

The new data are analyzed in two steps: given the presence of forbidden reflections, a model in the noncentrosymmetric, monoclinic space group $P2_1$ (a maximal subgroup of $P2_1/c$) was first developed (section 3.1); in a second step the superstructure reflections were interpreted in terms of the noncentrosymmetric, triclinic space group $A1$ (section 3.2). The disorder characteristics of CNS crystals are subtle, thus requiring unusually detailed experimental work and data analysis. We have investigated (i) different crystals from the same crystallization batch, (ii) crystals from different crystallization experiments, (iii) five sections obtained by cutting a single needle-shaped crystal, and (iv) measurements from different radiation sources (Mo Kα, Cu Kα, synchrotron).

*To whom correspondence should be addressed. (J.H.) Phone: +41 (0)31 631 42 41. Fax: +41 (0)31 631 42 44. E-mail: juerg.hulliger@iac.unibe.ch; (H.-B.B.) Phone: +41 (0)31 631 42 82. Fax: +41 (0)31 631 39 96. E-mail: hans-beat.buergi@krist.unibe.ch.

## 2. Experimental Section

CNS was prepared and characterized as described previously.[4] Starting materials and byproducts of the synthesis − especially the (*cis*)-isomer of CNS − were found to be below the detection limits of $^1$H NMR spectroscopy and GC-MS analysis.

Yellow needle-shaped prisms of CNS for X-ray analysis were grown in glass vessels from benzene solution by slow solvent evaporation at room temperature. Typical crystal diameters were 0.1−0.2 mm, with a ratio diameter/length of about 1:20. Two crystals were selected from the same batch of crystallization and found to show sharp extinction of visible, linearly polarized light. From each of them, a terminal section was cut (samples bz I and bz II). Sample bz III was obtained from a different batch of crystallization. It is a middle piece of a crystal, which was cut into five slices, called slices 1−5 (Note that "bz III" and "slice 3" refer to the same specimen). After the crystals were cut, the samples still showed sharp extinction under polarized light. They were mounted on glass fibers with two-component epoxy resin. Their morphology was determined at room temperature on an Enraf Nonius CAD 4 diffractometer. The needles are bounded by four prismatic faces indexed as (011), $(0\bar{1}\bar{1})$, $(0\bar{1}1)$ and Figure 1.[5] For less than 20% of the crystals, a small fifth face (010) was observed. The small end faces were difficult to characterize, but are close to (100) and $(\bar{1}00)$.

Reflections intensities for bz I, bz II, and bz III were measured at 298(3) K on a Bruker SMART 1K diffractometer, with graphite-monochromated Mo Kα radiation ($\lambda$ = 0.71073 Å) in the $\omega$ scan mode (scan width $\Delta\omega$ = 0.3°, exposure time 60 s/frame for bz I and bz II, 120 s/frame for bz III) using the built-in hemisphere strategy. Sample bz III was additionally measured on a STOE image plate 2T diffractometer using Cu radiation ($\lambda$ = 1.54186 Å, bz III Cu). Data measured on the Bruker diffractometer were reduced with program Saint+[6] and corrected empirically for absorption (program Sadabs[7]); both scaling and determination of the error model were based on Laue class 2/*m*. Reflection intensities of slices 1, 2, 3, 4, and 5 were measured at 294(1) K with the Kuma 6-circle diffractometer of the Swiss-Norwegian Beamline (SNBL) at the European Synchrotron Radiation Facilities (ESRF, Grenoble), $\lambda$ = 0.7100(5) Å. The intensities were collected in the $\omega$ scan mode (scan width $\Delta\omega$ = 1°), exposure time 4 s/frame with overflow retakes, and exposure time 16 s/frame without retakes (except for slice 3 that had overflow frames retaken) using a hemisphere strategy. In order to improve the statistics in terms of redundancy and Friedel coverage (see below), the data sets from short and long exposures were merged. Data reduction for these synchrotron data sets with CrysalisPro (release 171.31.7[8]) was followed by an empirical absorption correction with

 Published on Web 12/16/2009 

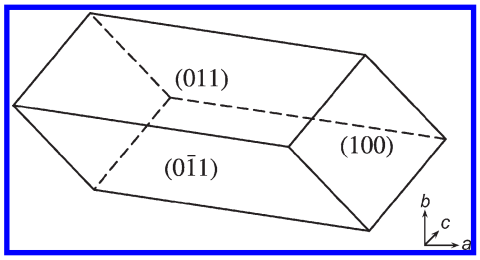


**Figure 1.** Morphology of the CNS needles with four prismatic faces. Only visible faces are indexed.[5]

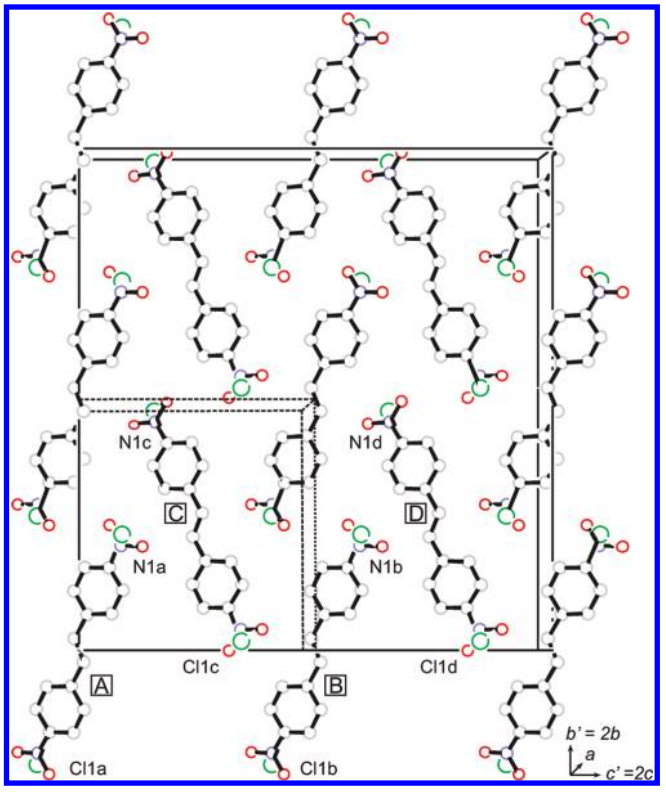


**Figure 2.** Projection along *a* of the structural model of CNS in space groups $P2_1$ (unit cell dashed) and $A1$. In the small unit cell molecules A and C are related to B and D by one *c*-translation; molecules A and B are related to C and D by a 2-fold screw operation along *b* (screw component *b*/2).

both scaling and error model assuming again Laue class 2/*m* (Sadabs[7]). As the superstructure reflections have significantly weaker intensities than the main ones, both classes of reflections were first processed separately in order to determine their respective resolution limits. The main and superstructure reflections were then combined, scaled, and corrected for absorption.

### 3. Results and Discussion

The consequences of the new diffraction data on the crystal structure are best summarized with reference to Figure 2, which shows the molecular packing projected onto the *b*,*c*-plane. In the original $P2_1/c$ structure, all molecular sites A, B, C, and D are occupied with identical molecules showing orientational disorder with the "up" and "down" orientations of the CNS molecule equally probable; that is, $p_{up} = p = 0.5$ and $p_{down} = 1 - p = 0.5$. Observable reflection intensities $I(h\ 0\ l)$ with *l* odd argue against a *c* glide plane and imply a symmetry lowering from $P2_1/c$ to the isotranslational maximal subgroup $P2_1$ (Figure 3). All molecular sites remain

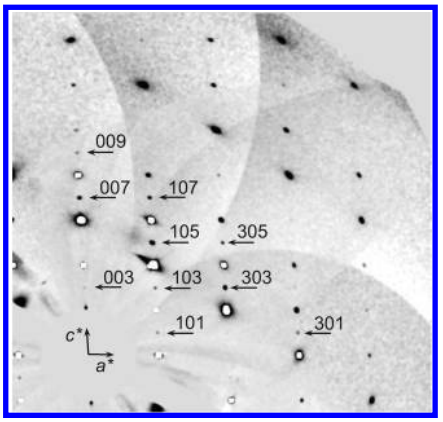


**Figure 3.** Reconstruction of (*h*0*l*) layer with the most prominent reflections violating $P2_1/c$ symmetry (arrows). The long exposure time necessary to show the violating reflections led to saturation of the allowed reflections (white in the center).

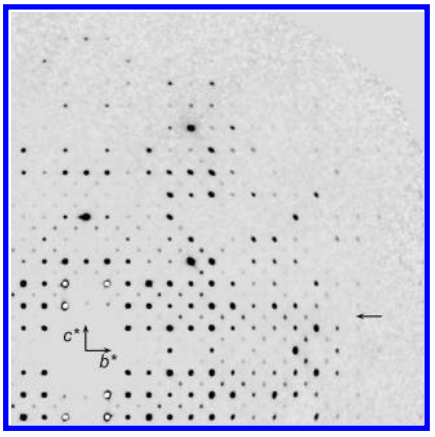


**Figure 4.** Reconstruction of (0*kl*) layer exhibiting both strong main reflections and weaker super structure reflections (one row indicated by an arrow).

identical, but $p \neq 0.5$. Because of the loss of the inversion center, inversion twins become possible. Their volume fractions may differ: $V_1 \neq V_{\bar{1}} \neq 0.5$. Further loss of the $2_1$ screw axis leads to a structure with the isotranslational maximal subgroup $P1$. Sites A and B are translation equivalent, as are sites C and D. The populations $p_A$ and $p_C$ are now different, but fulfill the condition $p_A(P1) + p_C(P1) = 2p(P2_1)$. Rotation twins with respect to the 2-fold axis and inversion twins are possible leading to twin elements 1, $\bar{1}$, 2, and *m* with the possibility that all volume fractions $V_1$,$V_{\bar{1}}$,$V_2$ and $V_m$ may differ. This structure has not been observed. Finally, the observation of superstructure reflection $I(h\ k{+}1/2\ l{+}1/2)$ implies a doubling of the unit cell parameters *b* and *c* and a centering translation in the *b*,*c*-plane, that is, space group $A1$. (Figure 4; the nonstandard setting $A1$ was chosen for easier comparison with the standard monoclinic setting used for the small unit cell). All four sites A, B, C, and D are now inequivalent with different populations $p_A$, $p_B$, $p_C$, $p_D$. The intensities of the main reflections depend on the averages $(p_A + p_B)/2 = p_A(P1)$ and $(p_C + p_D)/2 = p_C(P1)$; the intensities of the new superstructure reflections depend on the differences $(p_A - p_B)$ and $(p_C - p_D)$. Note that $(p_A + p_B + p_C + p_D)/4 = p(P2_1)$. No new twin domains arise. More detail is given in the Supporting Information. Throughout the analysis, it has been assumed that all molecules on all

sites are identical and are oriented as in the $P2_1/c$ model. The different population ratios imply differences in intermolecular interactions which might invalidate this approximation. However, such differences appear too small to be detected by least-squares refinements based on the available data.

**3.1. Refinement of a Structural Model in Space Group $P2_1$ from the Main Reflections.** The structures were refined on $F^2$ by least-squares methods with the SHELXTL suite of programs.[9] The resolution of reflection intensities included in the least-squares calculation for bz I, bz II, bz III, and bz III Cu are 0.76, 0.77, 0.76, and 0.90 Å, respectively. For the synchrotron data (slices 1−5), the resolution limit was set to 0.80 Å after careful inspection of the dependence of $R_{int}$ and $R_{sigma}$ on resolution as obtained from program Sadabs.[7] The asymmetric unit was assumed to contain a complete carbon skeleton, substituted in 4- and 4′-positions with *both* a chloro- and a nitro-substituent, each with partial occupancy. The coordinates and anisotropic displacement parameters (ADPs) of all non-H atoms have been refined under the constraint of local inversion symmetry to avoid excessive parameter correlation. The Cl atom on one side has a site occupation factor (SOF) $p$, the $NO_2$-group on the same side $(1 - p)$. The refinement of $p$ is thus based exclusively on the resolved electron density attributable to these substituents. H-atoms were refined as isotropic and riding. A ShelXtl instruction file for this model is given in the Supporting Information (Listing 3). Figure 5a represents the anisotropic displacement parameters and displays the atom numbering scheme employed in the structural model.[10] Crystal data, refinement statistics, and SOFs are summarized in Table 1 for all data sets.

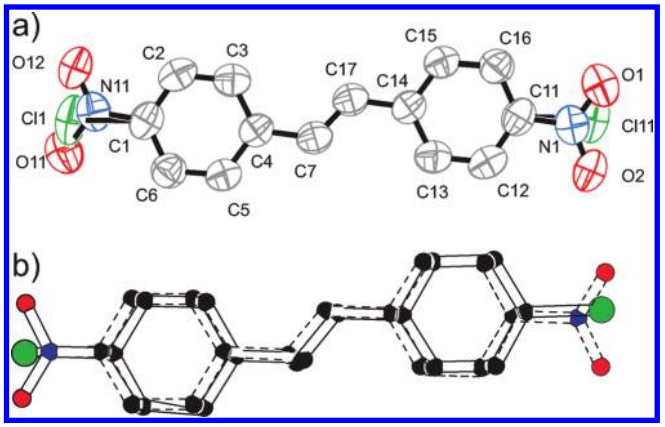


**Figure 5.** (a) Structural model with a single carbon skeleton decorated with disordered substituents at either end, atomic numbering scheme, and atomic displacement parameters (drawn at 50% probability level).[10] (b) Schematic representation of the superposition of two disordered CNS molecules (compare to Figure 2a).[10]

The deviation of $p$ from 0.5 is small but significant, thus confirming the lack of a center of inversion in the average crystal structure. The superiority of a description in the lower symmetry $P2_1$ over the one in $P2_1/c$ also follows from a refinement with $p$ fixed to 0.5 while keeping all other parameters (including the weighting scheme) unchanged: $wR2$ for the $P2_1/c$ model is 1−2% larger than for the $P2_1$-model (cf. Table 1). The significance of this improvement was

**Table 1. Results of the Least-Squares Refinement in Space Group $P2_1$ Based on the Main reflections[a]**

| sample | bz I | | bz II | | bz III[b] | | bz III Cu[b,c] | |
|---|---|---|---|---|---|---|---|---|
| structural model | $P2_1$ | $P2_1/c$ | $P2_1$ | $P2_1/c$ | $P2_1$ | $P2_1/c$ | $P2_1$ | $P2_1/c$ |
| $p$ | 0.427(3) | 0.500 | 0.431(3) | 0.500 | 0.431(3) | 0.500 | 0.432(3) | 0.500 |
| Flack parameter | −0.24(26) | | −0.31(27) | | −0.11(27) | | 0.26(7) | |
| $y$-parameter | 0.50(19) | | 0.69(16) | | 0.27(14) | | 0.35(4) | |
| reflections collected | 3470 | | 3473 | | 3445 | | 1754 | |
| unique reflections | 1865 | | 1870 | | 2296 | | 1516 | |
| unique reflections ($I > 2\sigma(I)$) | 921 | | 1067 | | 1362 | | 1021 | |
| $R_{int}$[d] | 0.015 | | 0.012 | | 0.015 | | 0.078 | |
| $R_{sigma}$[d] | 0.027 | | 0.020 | | 0.026 | | 0.051 | |
| $R_1$ ($I > 2\sigma(I)$)[d] | 0.043 | 0.046 | 0.042 | 0.045 | 0.054 | 0.057 | 0.045 | 0.049 |
| $R_1$ (all reflections)[d] | 0.110 | 0.114 | 0.088 | 0.092 | 0.097 | 0.100 | 0.064 | 0.070 |
| $wR_2$[d] | 0.116 | 0.124 | 0.114 | 0.123 | 0.126 | 0.133 | 0.107 | 0.117 |
| $S$ | 0.910 | 1.036 | 0.979 | 1.060 | 1.031 | 1.087 | 1.048 | 1.148 |
| $\Delta\rho_{max}$ (e Å$^{-3}$) | 0.10 | 0.10 | 0.11 | 0.13 | 0.12 | 0.13 | 0.15 | 0.15 |
| $\Delta\rho_{min}$ (e Å$^{-3}$) | −0.09 | −0.09 | −0.09 | −0.09 | −0.11 | −0.12 | −0.09 | −0.09 |

| sample | slice 1 | | slice 2 | | slice 3[b] | | slice 4 | | slice 5 | |
|---|---|---|---|---|---|---|---|---|---|---|
| structural model | $P2_1$ | $P2_1/c$ | $P2_1$ | $P2_1/c$ | $P2_1$ | $P2_1/c$ | $P2_1$ | $P2_1/c$ | $P2_1$ | $P2_1/c$ |
| $p$ | 0.449(2) | 0.500 | 0.444(2) | 0.500 | 0.440(2) | 0.500 | 0.438(2) | 0.500 | 0.437(2) | 0.500 |
| Flack parameter | 0.48(47) | | 0.31(16) | | 0.37(15) | | 0.36(16) | | 0.34(16) | |
| $y$-parameter | 0.34(3) | | 0.28(3) | | 0.37(2) | | 0.28(3) | | 0.29(3) | |
| reflections collected | 7590 | | 7461 | | 7983 | | 7410 | | 7483 | |
| unique reflections | 2464 | | 2478 | | 2497 | | 2487 | | 2485 | |
| unique reflections ($I > 2\sigma(I)$) | 1917 | | 2057 | | 2097 | | 2048 | | 1962 | |
| $R_{int}$[d] | 0.034 | | 0.027 | | 0.032 | | 0.026 | | 0.030 | |
| $R_{sigma}$[d] | 0.048 | | 0.033 | | 0.033 | | 0.031 | | 0.033 | |
| $R_1$ ($I > 2\sigma(I)$)[d] | 0.048 | 0.050 | 0.043 | 0.046 | 0.046 | 0.048 | 0.045 | 0.049 | 0.045 | 0.048 |
| $R_1$ (all reflections)[d] | 0.059 | 0.061 | 0.051 | 0.054 | 0.053 | 0.055 | 0.053 | 0.057 | 0.054 | 0.058 |
| $wR_2$[d] | 0.152 | 0.175 | 0.122 | 0.147 | 0.134 | 0.158 | 0.136 | 0.168 | 0.127 | 0.155 |
| $S$ | 0.877 | 1.011 | 0.938 | 1.128 | 1.061 | 1.246 | 0.933 | 1.150 | 0.913 | 1.112 |
| $\Delta\rho_{max}$ (e Å$^{-3}$) | 0.23 | 0.17 | 0.12 | 0.12 | 0.24 | 0.20 | 0.13 | 0.12 | 0.16 | 0.11 |
| $\Delta\rho_{min}$ (e Å$^{-3}$) | −0.15 | −0.14 | −0.12 | −0.12 | −0.14 | −0.15 | −0.13 | −0.12 | −0.12 | −0.12 |

[a] The column entitled $P2_1/c$ refers to the same model with the same weighting scheme, but with $p$ constrained to 0.5. [b] Samples bz III, bz III Cu, and slice 3 are the same crystal. [c] Sealed tube, Cu Kα, $\lambda$ = 1.54186 Å, resolution limit of 0.9 Å. [d] $R_{int} = \sum|F_o^2 - \bar{F}_o^2|/\sum F_o^2$, $R_{sigma} = \sum[\sigma(F_o^2)]/\sum F_o^2$, $R_1 = \sum||F_o| - |F_c||/\sum|F_o|$, $wR_2 = (\sum[w(F_o^2 - F_c^2)^2]/\sum[w(F_o^2)^2])^{1/2}$, GOF = $S = (\sum[w(F_o^2 - F_c^2)^2]/(n - p))^{1/2}$.

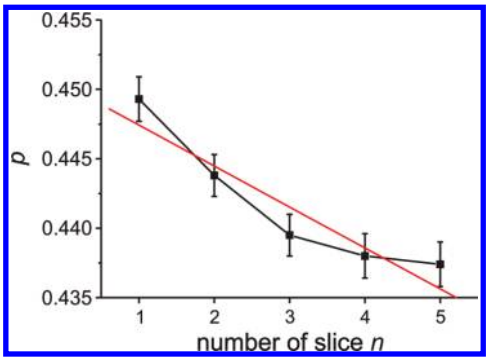


**Figure 6.** $p$'s for slices 1−5. $p = 0.450(2) - 0.0030(5)\,n$, $R^2 = 0.88$ (Table 1). Small unit cell, $P2_1$-model.

statistically validated by an $R$-factor ratio test (Supporting Information, Table S2).[11]

Comparison of the converged SOFs shows that the small deviations from 0.5 are reproducible (cf. Table 1). They do not depend on the crystal specimen, nor on the crystallization batch, nor on the diffractometer, nor on the radiation used (Mo Kα, Cu Kα, synchrotron). With an average $p$ of 0.437(7), these samples are definitely not centrosymmetric. A weak tendency for $p$ to decrease from slice 1 to 5, with a maximum difference $p$(slice 1) − $p$(slice 5) of 0.012(3), cannot be excluded entirely (cf. Figure 6).

The presence of inversion twinning involving crystal domains of opposite polarity (and chirality) may be gauged in principle from the Flack parameter.[12] For all samples investigated with Mo radiation, this parameter is poorly determined. Standard uncertainties (s.u.) are large due to the small anomalous scattering power of chlorine atoms for Mo radiation and to the fact that the difference in population between the two disordered Cl atoms is only about 0.15 (Table 1). The experiment on bz III with Cu radiation resulted in a physically meaningful, positive Flack parameter with a small s.u. in contrast to the one from the experiment on bz III with Mo radiation. An alternative to the Flack parameter is the $y$-parameter recently proposed.[13] While the former is derived from whatever Bragg intensities have been measured, the latter relies exclusively on intensity differences between Friedel pairs, $I(hkl) - I(\overline{hkl})$, and thus on the percentage of reflections for which such pairs have been measured. The so-called Friedel coverage is 64% (bz I and II), 79% (bz III), 85% (bz III Cu), and 97 to 98% for slices 1−5, respectively. Corresponding $y$-parameters have been calculated[13] and are compared to Flack parameters (cf. Table 1). In spite of limited coverage all $y$'s are within the physically meaningful range between 0 and 1 unlike the Flack parameters for bz I, bz II, and bz III. In addition their s.u.'s are smaller. For slices 1−5 with nearly complete Friedel coverage the $y$'s are well determined, consistent between slices, and there is also agreement between bz III Cu and slice 3 (representing different measurements on the same sample). Overall, the results on the $y$-parameters indicate inversion twinning with unequal volume fractions of the two domains. Measurements complementary to single crystal X-ray crystallography such as phase sensitive second harmonic generation (PS-SHG)[14] and more recently scanning pyroelectric microscopy (SPEM)[4] have provided independent evidence that the structure is inversion twinned. Theoretical work on this material points in the same direction.[15]

Some remarks on bond lengths and cell constants are in order. Two bond lengths in our model differ considerably from reference values: $d$(C11−Cl) is in the range 1.867(2) to 1.877(5) Å, whereas the reference value is shorter, 1.739(10) Å; $d$(C11-$NO_2$) is in the range 1.340(6) to 1.384(8) Å to be compared to a reference value which is longer, 1.468(14) Å.[16] The same observation has been reported for 4-chloro-nitrobenzene.[17] Both incongruities are easily explained in terms of two antiparallel molecules whose carbon skeletons are shifted by ∼0.1 Å relative to each other along the long molecular axis and show normal $d$(C11−Cl) and $d$-(C11−$NO_2$) distances, as depicted in Figure 5b. As the shift is much below the resolution limit of the data, the positional disorder in the carbon skeleton had to be modeled by a single, centrosymmetric carbon frame in average position and with unit SOF; the carbon disorder results in slightly elongated anisotropic displacement parameters and explains the deviant bond lengths.

This diffraction analysis confirms the cell constants of the crystal structure reported previously.[2] The results reported in Table S1 are based on nine diffraction measurements from seven different samples. The accuracy of the results derived from the population variance of these routine measurements is about an order of magnitude inferior to the s.u. of individual cell determinations.[18]

**3.2. Refinement of a Structural Model from the Main and Superstructure Reflections. 3.2.1. Statistical Analysis of Main and Superstructure Reflections.** The diffraction data were reintegrated in the enlarged unit cell $a' = a$, $b' = 2b$, $c' = 2c$, assumed as primitive and the following reflection classes analyzed statistically: $k' = 2n + 1$ and $l' = 2n$ ($k_o' l_e'$); $k' = 2n$ and $l' = 2n + 1$ ($k_e' l_o'$); $k' = 2n + 1$ and $l' = 2n + 1$ ($k_o' l_o'$); $k' = 2n$ and $l' = 2n$ ($k_e' l_e'$).

The results confirm $A$-centering. Figure 7 emphasizes the different characteristics of the $I/\sigma(I)$-distributions of parities $k_o' l_o'$ and $k_o' l_e'$ (drawn after removal of a few outliers outside the intervals of $-5 \le I/\sigma(I) \le +5$ and $-5 \le I/\sigma(I)$, respectively, in each case much less than 1% of the total number of reflections; cf. Supporting Information, Table S3). As shown in Figure 7, the distribution $k_o' l_e'$ is smoothly approximated by a Gaussian centered at zero indicating an expectation value $\langle I(k_o' l_e')\rangle = 0$. For reflection class $k_o' l_o'$, the corresponding histogram clearly differs: it shows a non-Gaussian distribution with a tail toward positive values of $I/\sigma(I)$, indicating the presence of significant superstructure reflections. Analogous conclusions apply to reflections of type $k_e' l_o'$ (behaving like $k_o' l_e'$) and $k_e' l_e'$ (similar to $k_o' l_o'$), respectively.

The visual interpretation of the $I/\sigma(I)$-distributions was further validated by numerical statistics. For the parities $k_o' l_e'$ and $k_e' l_o'$, the arithmetical means and skewnesses are nearly zero, the standard deviations are close to one, and the kurtosis is small indicating a normal distribution of $I/\sigma(I)$ with mean 0 and variance 1. In contrast to this result, tails on the positive side of the distributions for reflection classes $k_o' l_o'$ and $k_e' l_e'$ imply positive mean and median, an increased standard deviation and a nonzero skewness (Supporting Information, Table S3). Thus, both the presence of superstructure reflections and the $A$-centering in question were confirmed.

Given the relatively weak intensities of the $k_o' l_o'$ reflections, a resolution limit lower than that of the $k_e' l_e'$ reflections was defined: the quantities $I/\sigma(I)$ were drawn separately as a function of $d^{*2} = (2 \sin\theta/\lambda)^2$ for the populations $k_e' l_e'$ and $k_o' l_o'$ of samples bz I, bz II, bz III; after visual inspection the resolution limits were set at 0.80 Å for $k_e' l_e'$

**Table 2. Some Results from the Least-Square Refinements Based on the Main and Superstructure Reflections**

| sample | bz I | bz II | bz III[a] | bz III Cu[a,b] |
|---|---|---|---|---|
| $p_A$ | 0.513(11) | 0.522(10) | 0.365(57) | 0.520(40) |
| $p_B$ | 0.379(11) | 0.379(10) | 0.548(57) | 0.417(40) |
| $p_C$ | 0.555(7) | 0.564(7) | 0.610(25) | 0.649(11) |
| $p_D$ | 0.247(7) | 0.244(7) | 0.183(25) | 0.162(11) |
| $<p>$ [rms] | 0.424 (0.121) | 0.427 (0.126) | 0.427 (0.167) | 0.437 (0.179) |
| $p(P2_1)$[c] | 0.427(3) | 0.431(3) | 0.431(3) | 0.432(3) |
| $V_1$ | 0.368(14) | 0.379(12) | 0.479(12) | 0.467(10) |
| Flack parameter | −0.5(3) | −0.4(3) | −0.3(4) | 0.3(1) |
| | | Main and Superstructure Reflections | | |
| reflections integrated | 4459 | 4465 | 4431 | 5308 |
| unique reflections | 3602 | 3612 | 3585 | 3145 |
| unique reflections ($I > 2\sigma(I)$) | 1746 | 2046 | 2216 | 2031 |
| $R_{int}$ | 0.014 | 0.012 | 0.016 | 0.080 |
| $R_{sigma}$ | 0.033 | 0.026 | 0.034 | 0.062 |
| $R_1$ ($I > 2\sigma(I)$) | 0.058 | 0.059 | 0.081 | 0.090 |
| $R_1$ (all reflections) | 0.131 | 0.109 | 0.124 | 0.117 |
| $wR_2$ | 0.122 | 0.128 | 0.156 | 0.248 |
| $S$ | 1.074 | 1.100 | 1.117 | 1.152 |
| $\Delta\rho_{max}$ (e Å$^{-3}$) | 0.16 | 0.18 | 0.22 | 0.20 |
| $\Delta\rho_{min}$ (e Å$^{-3}$) | −0.16 | −0.13 | −0.21 | −0.19 |
| | | Main Reflections Only | | |
| reflections integrated | 3395 | 3399 | 3371 | 2933 |
| unique reflections | 2841 | 2846 | 2816 | 1796 |
| unique reflections ($I > 2\sigma(I)$) | 1426 | 1634 | 1661 | 1318 |
| $R_{int}$ | 0.013 | 0.011 | 0.014 | 0.078 |
| $R_{sigma}$ | 0.031 | 0.024 | 0.032 | 0.052 |
| $R_1$ ($I > 2\sigma(I)$) | 0.046 | 0.046 | 0.062 | 0.055 |
| $R_1$ ($I > 2\sigma(I)$) ($P2_1$)[c] | 0.043 | 0.042 | 0.054 | 0.045 |
| $R_1$ (all reflections) | 0.111 | 0.090 | 0.105 | 0.069 |
| $wR_2$ | 0.095 | 0.099 | 0.120 | 0.139 |
| $S$ | 0.937 | 0.949 | 0.955 | 0.803 |
| | | Superstructure Reflections Only | | |
| reflections integrated | 1064 | 1066 | 1060 | 2375 |
| unique reflections | 761 | 766 | 769 | 1349 |
| unique reflections ($I > 2\sigma(I)$) | 320 | 412 | 555 | 713 |
| $R_{int}$ | 0.208 | 0.158 | 0.081 | 0.121 |
| $R_{sigma}$ | 0.418 | 0.295 | 0.174 | 0.253 |
| $R_1$ ($I > 2\sigma(I)$) | 0.258 | 0.247 | 0.241 | 0.265 |
| $R_1$ (all reflections) | 0.394 | 0.334 | 0.284 | 0.308 |
| $wR_2$ | 0.591 | 0.551 | 0.539 | 0.580 |
| $S$ | 1.543 | 1.604 | 1.644 | 1.524 |

| sample | slice 1 | slice 2 | slice 3[a] | slice 4 | slice 5 |
|---|---|---|---|---|---|
| $p_A$ | 0.514(10) | 0.505(14) | 0.381(26) | 0.542(22) | 0.522(22) |
| $p_B$ | 0.446(10) | 0.431(14) | 0.439(26) | 0.391(22) | 0.406(22) |
| $p_C$ | 0.616(3) | 0.647(5) | 0.689(5) | 0.582(11) | 0.600(8) |
| $p_D$ | 0.231(3) | 0.204(5) | 0.242(5) | 0.248(11) | 0.231(8) |
| $<p>$ [rms] | 0.452 (0.141) | 0.447 (0.160) | 0.438 (0.162) | 0.441 (0.132) | 0.440 (0.139) |
| $p(P2_1)$[c] | 0.449(2) | 0.444(2) | 0.440(2) | 0.438(2) | 0.437(2) |
| $V_1$ | 0.424(7) | 0.442(8) | 0.472(7) | 0.474(7) | 0.470(7) |
| Flack parameter | 0.4(2) | 0.3(3) | 0.1(2) | 0.3(3) | 0.3(3) |
| | | Main and Superstructure Reflections | | | |
| reflections integrated | 13419 | 13434 | 13989 | 13395 | 13422 |
| unique reflections | 7324 | 7400 | 7386 | 8825 | 8805 |
| unique reflections ($I > 2\sigma(I)$) | 4374 | 5018 | 5527 | 5589 | 5280 |
| $R_{int}$ | 0.054 | 0.042 | 0.042 | 0.038 | 0.038 |
| $R_{sigma}$ | 0.061 | 0.056 | 0.056 | 0.062 | 0.064 |
| $R_1$ ($I > 2\sigma(I)$) | 0.085 | 0.088 | 0.092 | 0.086 | 0.085 |
| $R_1$ (all reflections) | 0.110 | 0.106 | 0.105 | 0.111 | 0.115 |
| $wR_2$ | 0.318 | 0.269 | 0.281 | 0.284 | 0.275 |
| $S$ | 1.443 | 1.219 | 1.484 | 1.185 | 1.216 |
| $\Delta\rho_{max}$ (e Å$^{-3}$) | 0.36 | 0.34 | 0.36 | 0.31 | 0.34 |
| $\Delta\rho_{min}$ (e Å$^{-3}$) | −0.20 | −0.22 | −0.24 | −0.18 | −0.19 |
| | | Main Reflections Only | | | |
| reflections integrated | 7627 | 7527 | 7982 | 7440 | 7512 |
| unique reflections | 3684 | 3713 | 3690 | 4823 | 4826 |
| unique reflections ($I > 2\sigma(I)$) | 2714 | 2934 | 3102 | 3539 | 3356 |
| $R_{int}$ | 0.048 | 0.038 | 0.040 | 0.031 | 0.031 |
| $R_{sigma}$ | 0.059 | 0.054 | 0.055 | 0.059 | 0.061 |
| $R_1$ ($I > 2\sigma(I)$) | 0.051 | 0.046 | 0.045 | 0.051 | 0.050 |
| $R_1$ ($I > 2\sigma(I)$) ($P2_1$)[c] | 0.048 | 0.043 | 0.046 | 0.045 | 0.045 |
| $R_1$ (all reflections) | 0.062 | 0.054 | 0.052 | 0.066 | 0.070 |

**Table 2. Continued**

| sample | slice 1 | slice 2 | slice 3[a] | slice 4 | slice 5 |
|---|---|---|---|---|---|
| $wR_2$ | 0.155 | 0.122 | 0.121 | 0.152 | 0.145 |
| $S$ | 0.887 | 0.723 | 0.821 | 0.792 | 0.801 |
| | | | Superstructure Reflections Only | | |
| reflections integrated | 5792 | 5907 | 6007 | 5955 | 5910 |
| unique reflections | 3640 | 3687 | 3696 | 4002 | 3979 |
| unique reflections ($I > 2\sigma(I)$) | 1660 | 2084 | 2425 | 2050 | 1924 |
| $R_{int}$ | 0.142 | 0.080 | 0.075 | 0.120 | 0.119 |
| $R_{sigma}$ | 0.187 | 0.116 | 0.091 | 0.163 | 0.166 |
| $R_1$ ($I > 2\sigma(I)$) | 0.290 | 0.287 | 0.292 | 0.295 | 0.291 |
| $R_1$ (all reflections) | 0.346 | 0.328 | 0.322 | 0.345 | 0.340 |
| $wR_2$ | 0.625 | 0.611 | 0.610 | 0.626 | 0.625 |
| $S$ | 1.854 | 1.577 | 1.942 | 1.539 | 1.590 |

[a] Samples bz III, bz III Cu and slice 3 are the same crystal. [b] Sealed tube, Cu Kα, $\lambda$ = 1.54186 Å. [c] From Table 1.

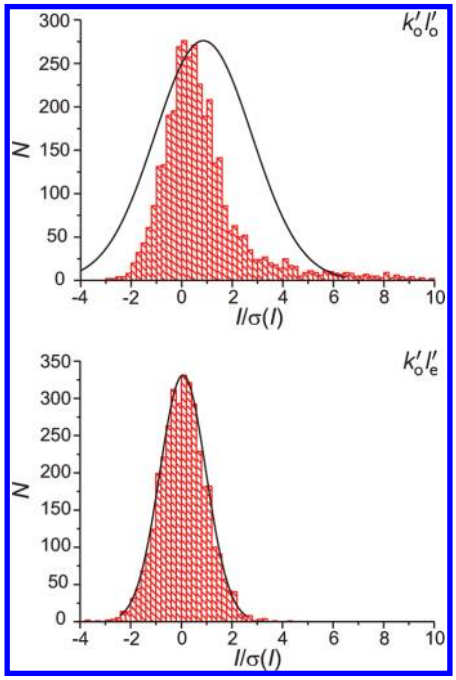


**Figure 7.** Histograms for the two reflections classes $k_o'\,l_o'$ and $k_o'\,l_e'$ of sample bz I (red bars) compared to Gaussian distributions (black envelope) based on sample means and standard deviations.

and 1.30 Å for $k_o'\,l_o'$, respectively (cf. Figure 8). Using the same approach, the data for bz III Cu − measured with Cu radiation − were restricted to 0.90 Å and 1.05 Å, respectively. For the synchrotron data sets of slices 1−5 a resolution limit of 0.80 Å was determined for the data $k_e'\,l_e'$ from short and long exposures as well as for the data $k_o'\,l_o'$ from the long exposure; but a limit of 1.10 Å was chosen for $k_o'\,l_o'$ from the short exposure.

Samples bz I, bz II, and bz III were reintegrated to high resolution to obtain the main reflections intensities and to lower resolution to obtain the superstructure reflection intensities. In both cases, the same integration parameters were chosen to ascertain a comparable basis for scaling. Subsequent to numerical absorption correction of the complete data set bz III Cu, the individual resolution limits of its separated parities $k_e'\,l_e'$ and $k_o'\,l_o'$ were determined with Xprep.[19] Synchrotron data sets of slices 1−5 were treated with the Crysalis software,[8] which allows one to limit the resolution in the final part of the integration and to produce separate *hkl*-files at the chosen resolution limits for reflection classes $k_e'\,l_e'$ and $k_o'\,l_o'$. A final *hkl*-file was then created, for each specimen, by merging hkl-files $k_e'\,l_e'$ and $k_o'\,l_o'$. The data were corrected for absorption with Sadabs, assuming Laue symmetry 2/*m* for scaling and error model.[7]

**3.2.2. Refinement Model.** Doubling the cell constants *b* and *c* and lowering the space group symmetry to *A*1 increases the content of the asymmetric unit from one site containing a pair of disordered molecules with unequal population to four such sites with independent SOFs $p_A$, $p_B$, $p_C$, $p_D$ (Figure 2). Atomic coordinates were derived from the corresponding $P2_1$ model and kept fixed (Supporting Information, Listing 4). Molecules A and C are thus related to molecules B and D by the noncrystallographic translation $c'/2$, molecules A and B are related to molecules C and D by noncrystallographic screw rotations $2_{1/2}$ parallel to $b'$ at $^1/_8$, $^3/_8$, $^5/_8$, and $^7/_8$ $c'$. The same anisotropic ADPs were applied to corresponding atoms in all four molecules and refined as free variables (Supporting Information, Listing 4).

The volume fractions of the two twin domains related by the 2-fold axes have been introduced into the model explicitly as $V_1$ and $V_2 = 1 - V_1$ and refined during the least-squares calculations. The low anomalous dispersion of Cl for Mo-radiation again prohibits accurate determination of Flack parameters and thus of inversion twinning, that is, of $V_{\bar{1}}$ and $V_m$; the latter have not been included in the model to avoid excessive parameter correlation. It is likely, however, that inversion twinning for the *A*1-model is similar to that of the $P2_1$-model. Friedel coverage is too low (28−48%) to calculate meaningful *y*-parameters. Refinement results are provided in Table 2.

The intensities of the main reflections $k_e'\,l_e'$ are larger on average than those of the superstructure reflections $k_o'\,l_o'$ and therefore more accurate than the latter. In order to estimate how well the structural model explains the two different reflection classes, separate *R*-values were calculated for the two parity classes (Table S5). $R(k_e'\,l_e')$ for the *A*1-model is only marginally lower than that for the $P2_1$-model. $R(k_o'\,l_o')$'s are generally higher as expected from the internal consistency $R_{int}$ of equivalent reflection and from their accuracy $R_{sigma}$. The quantity $wR2$ and the goodness-of-fit statistic *S* of the superstructure reflections show analogous differences indicating that the weights of this reflection class are underestimated. The preference for the *A*1-model over the pseudo $P2_1$ structure is nevertheless obvious: while the former requires the presence of the superstructure reflections $k_o'\,l_o'$, the latter requires the superstructure intensities to be zero, contrary to observation.

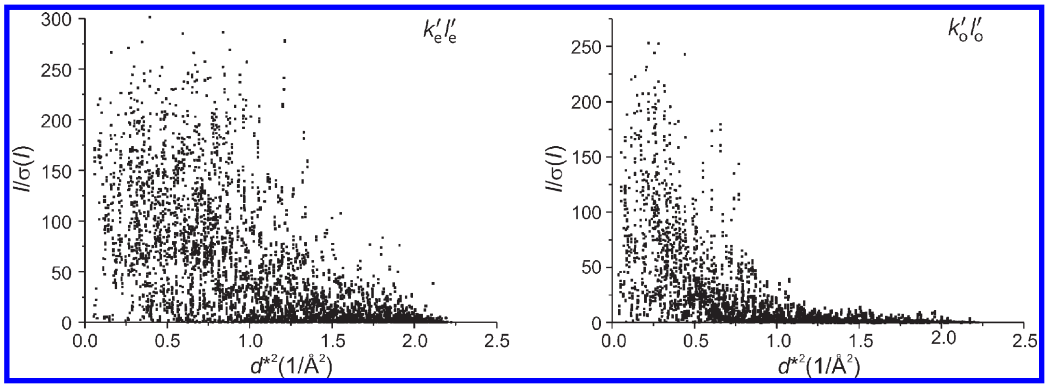


**Figure 8.** Typical $I/\sigma(I)$ distributions for main ($k_e' l_e'$) and superstructure reflections ($k_o' l_o'$) drawn as a function of the reciprocal resolution $(2\sin\theta/\lambda)^2$ (slice 3, long exposure). From such plots the limits of resolutions of the different parities were determined by visual inspection (see text).

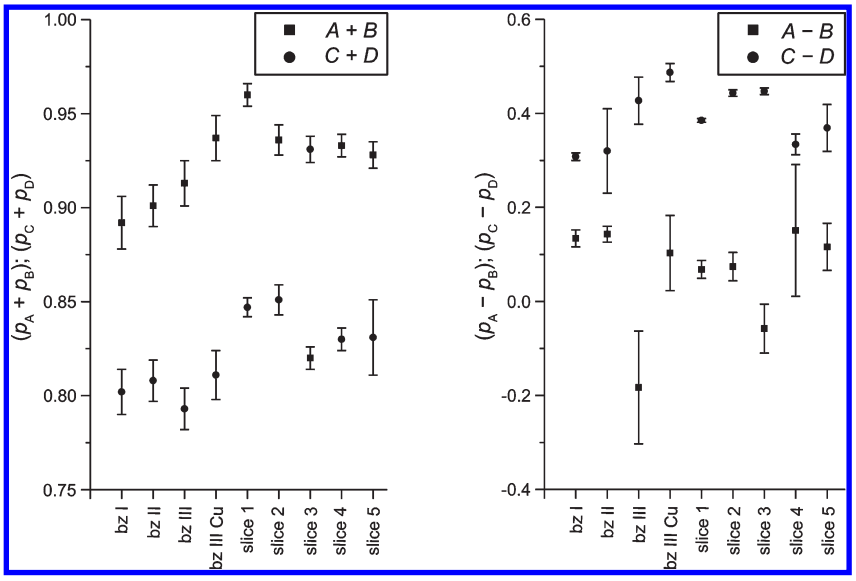


**Figure 9.** Sums and differences $(p_A + p_B)$, $(p_C + p_D)$, $(p_A - p_B)$, and $(p_C - p_D)$, for the various specimens and experiments.

Given the intensity differences between main and superstructure reflections and the fact that $(p_A + p_B)$ and $(p_C + p_D)$ are determined by the main reflections, whereas $(p_A - p_B)$ and $(p_C - p_D)$ depend on the superstructure reflections, the interpretation of $p_A, p_B, p_C, p_D$ requires considering not only their refined values, but also their s.u.'s (Table 2) and correlation coefficients (Supporting Information, Table S4). For some experiments, the latter vary widely and may be as large as 0.98. The sums of populations are generally better determined than their differences (Supporting Information, Table S6). Figure 9 shows the sums $(p_A + p_B)$ and $(p_C + p_D)$ to be fairly constant at ~0.9 and 0.8, whereas the differences $(p_A - p_B)$ and $(p_C - p_D)$ are much smaller and tend to be less well determined. The differences $(p_A - p_B)$ for the two experiments bz III and slice 3 (Mo K$\alpha$ and synchrotron radiation, same crystal) are noteworthy because they are opposite in sign compared to all other experiments; in addition their s.u.'s are large. A structure factor calculation with $p_A$ and $p_B$ interchanged results in *R*-factors that are insignificantly different ($p_A$ and $p_B$ from Table 2: $R1(I > 2\sigma(I)) = 0.0807$, $wR2 = 0.1560$, GOF = $S = 1.117$; $p_A$ and $p_B$ interchanged: $R1(I > 2\sigma(I)) = 0.0809$, $wR2 = 0.1562$, $S = 1.119$). This observation can be traced to the 2-fold twinning of the sample. An algebraic analysis of the diffraction intensities for the weak reflections shows that for a twin ratio of 1:1 ($V_1 = V_2 = 0.5$) the intensities of the superstructure reflections depend on $(p_A - p_B)^2$ and $(p_C - p_D)^2$ and are thus independent of the sign of the difference. Note that for bz III and slice 3 $V_1 \sim 0.48(1)$, close to 0.5 and that the *S*-values are highest (cf. Supporting Information, analysis of the structure factor equation).

The above discussion has shown the scope and limitation of interpreting the special diffraction pattern of CNS with its strong main and weak superstructure reflections. In spite of some limitations, a firm conclusion can be drawn: The SOFs characterizing the twinned, triclinic superstructure of CNS obtained from nine experiments are mutually consistent; there appear to be no significant differences arising from crystallization batches, position of sample in a longish needle (slices 1−5) nor from the use of different radiation sources.

## 4. Summary and Conclusions

We have shown that the contradiction between the centrosymmetric structure of CNS previously claimed and some of its macroscopic properties requiring a noncentrosymmetric structure may be resolved by considering some subtle, but unambiguous features in the single crystal diffraction pattern. Some weak but significant diffraction intensities $I(h0l)$ all with $l$ odd indicate a violation of the glide symmetry $c$ and suggest a description of the average structure in space group $P2_1$, rather

than $P2_1/c$ (Figure 3). This hypothesis was confirmed by allowing two superimposed CNS molecules of opposite orientation to assume different populations $p$ and $(1 - p)$. The SOF's $p$ from nine different experiments are distributed about a mean of 0.437 with a population standard deviation of 0.007, a small, but significant deviation from 0.5.

Inspection of reciprocal space unveiled a set of additional, quite weak superstructure reflections requiring a doubling of the $b$ and $c$ axes and a structural model with at least 2-fold twinning in space group $A1$ (Figure 4). The triclinic unit cell contains four molecular sites, all of them occupied by two molecules of opposite orientation and different populations. Crystal growth seems to differentiate not only between molecular orientations in a single site, but does so in four different sites.

The monoclinic model reveals inversion twinning with unequal volume fractions. The triclinic model additionally entails 2-fold twinning about the original 2-fold axis. The occasional presence of an extra (010) face, but not of the corresponding $(0\bar{1}0)$ face, also indicates unequal volume fractions of the inversion twins.

In summary, the present study shows that (1) crystals of CNS are built from polar domains of unequal volumes (two types in the case of 2-fold twinning, four if inversion twinning is also present), and (2) the polarity of individual domains is due to a subtle, microscopic imbalance of molecular orientation arising during crystal growth. Experiments on specimens from different crystallization batches provide very comparable results. The small discrepancies between results from the same crystal investigated with different radiations indicate that the accuracy of results from different crystals is less than indicated by the precision, that is, s.u.'s, of the least-squares results. The present study addresses the average structure and cannot provide unambiguous information about local variations of orientational disorder in the fully grown crystals. Site occupation factors and twin ratios from a single crystal cut into five pieces of approximate dimension $0.2 \times 0.1 \times 0.1$ mm$^3$ do not show a convincing dependence on position in the original crystal. However, variations of site-occupation factors and twin ratios at lengths scale less than $\sim$0.1 mm cannot be excluded on the basis of the experiments presented here.

The unequal populations at the disordered sites and the unequal volume fractions of the twin domains imply an absence of local and global centers of inversion and are thus compatible with both second harmonic generation and pyroelectric effect, but do not lead to a quantitative understanding of these physical properties. In a follow-up paper, we will describe the influence of the solvent of crystallization on the disorder and twin structure of 4-chloro-4′-nitrostilbene and discuss the results on the background of materials with analogous properties.

We conclude with a remark on experimentation. The present reinvestigation of CNS was provoked by an inconsistency between the results of a routine diffraction experiment and a series of SHG and pyroelectric experiments.[2,4] The automated program packages used in the initial interpretation of the diffraction data missed two things: (1) some small, but significant deviations from a systematic absence rule and (2) a set of quite weak superstructure reflections. These features, although present in the CCD frames, have been spotted only after challenging the statistics on systematic absences and reconstructing the primary data in reciprocal space. The clearly laid-out geometry of such reconstructions allowed quick and thorough scrutiny for weak and unusual diffraction features. Once the true nature of the data was recognized, a range of related experiments could be interpreted with the help of today's automated, highly developed technology. Our experience uncovered the dangers of overnight crystal structure determinations and shows that the additional expenditure for reciprocal space reconstructions is well justified if subtle relationships between materials properties and atomic or molecular structure are at issue.

**Acknowledgment.** We thank Prof. Stoeckli-Evans for the initial determination of the structure of CNS, the staff of the Swiss-Norwegian Beamlines at ESRF for their untiring support and the referees for many valuable suggestions. The Swiss National Science Foundation (Project no. 200021-101658/1) and the Swiss NRP 47 Functional Supramolecular Materials (4047-057476/1) are acknowledged for financial support.

**Supporting Information Available:** $R$-factor ratio test of significance between the $P2_1$ models with $p$ refined freely and constrained to 0.5; statistical analysis of the main and superstructure reflections (cf. text). Some correlation coefficients from the least-squares refinement of the $A1$ model; sums and differences of populations with their s.u.'s in the $A1$ model; plot of $p$ for slices 1−5 with results of a linear regression, small unit cell, $P2_1$ model; plot of $p_A$, $p_B$, $p_C$, $p_D$ for the various specimens and experiments, big unit cell, $A1$ model; analysis of the structure factors equations for the structural model in space group $A1$; listing 2: ShelXtl instruction file for the least-squares refinement in space group $P2_1/c$ based on the main reflections; listing 3: ShelXtl instruction file for the least-squares refinement in space group $P2_1$ based on the main reflections; listing 4: ShelXtl instruction file for the least-squares refinement in space group $A1$ based on main and superstructure reflections; crystallographic information files (CIF). This material is available free of charge via the Internet at http://pubs.acs.org.

## References

(1) Wang, Y.; Tam, W.; Stevenson, S. H.; Clement, R. A.; Calabrese, J. *Chem. Phys. Lett*. **1988**, *148*, 136–141.
(2) Hulliger, J.; Bebie, H.; Kluge, S.; Quintel, A. *Chem. Mater*. **2002**, *14*, 1523–1529.
(3) Behrnd, N.-R.; Labat, G.; Venugopalan, P.; Hulliger, J.; Bürgi, H.-B., to be published.
(4) Behrnd, N.-R.; Couderc, G.; Wübbenhorst, M.; Hulliger, J. *Phys. Chem. Chem. Phys*. **2006**, *8*, 4132–4137.
(5) *SHAPE*, version V 7.2.1; Shape Software: Kingsport, USA, 2006.
(6) *SAINT+*, version 6.45; Bruker AXS Inc.: Madison, Wisconsin, USA, 2003.
(7) Sheldrick, G. M. *SADABS-2004/1*; Bruker AXS Inc.: Madison, Wisconsin, USA, 2004.
(8) *CrysalisPro*, version 171.31.7; Oxford Diffraction, 2006.
(9) Sheldrick, G. M. *SHELXTL*, version 6.14; Bruker AXS Inc.: Madison, Wisconsin, USA, 2000.
(10) (a) Spek, A. L. *PLATON* for Windows Taskbar v 1.10; University of Utrecht: The Netherlands, 2006. (b) Spek, A. L. *Acta Crystallogr*. **1990**, *A46*, C34. (c) Spek, A. L. *J. Appl. Crystallogr*. **2003**, *36*, 7–13. (d) Farrugia, L. *ORTEP-3* for Windows, J. *J. Appl. Cryst*. **1997**, *30*, 565.
(11) (a) Hamilton, W. C. In *Statistics in Physical Science*; The Ronald Press Company: New York, 1964; pp 157−160. (b) Hamilton, W. C. *Acta Crystallogr*. **1965**, *18*, 502–510.
(12) Flack, H. D. *Acta Crystallogr*. **1983**, *A39*, 876–881.
(13) Hooft, R. W. W.; Straver, L. H.; Spek, A. L. *J. Appl. Crystallogr*. **2008**, *41*, 96–103.
(14) Kluge, S.; Budde, F.; Dohnke, I.; Reichsteiner, P.; Hulliger, J. *Appl. Phys. Lett*. **2002**, *81*, 247–249.
(15) Gervais, C.; Wüst, T.; Behrnd, N.-R.; Wübbenhorst, M.; Hulliger, J. *Chem. Mater*. **2005**, *17*, 85–94.
(16) Allen, A. H.; Waston, D. G.; Brammer, L.; Orpen, A. G.; Taylor, R. In *International Tables for Crystallography*, 2nd ed.; Wilson, A. J. C.; Prince, E., Eds.; Kluwer Academic Publishers: Dordrecht, 1999; Vol. C: Mathematical, Physical and Chemical Tables, chapter 9.5, pp 793, 795.
(17) Thomas, L. H.; Cole, J. M.; Wilson, C. C. *Acta Crystallogr*. **2008**, *C64*, o296–o302.
(18) Herbstein, F. H. *Acta Crystallogr*. **2000**, *B56*, 547–557.
(19) *XPREP*, Version 6.14; Bruker AXS Inc.: Madison, Wisconsin, USA, 2001.